Supporting Information

Microbial Colonization of Chasmoendolithic Habitats in the Hyper-arid Zone of the Atacama Desert by DiRuggiero et al.

1. Experimental procedures

1.1 Sampling and site characterization

In 2010, rhyolite rocks of volcanic origin were collected in the Lomas de Tilocalar area, south of the Salar de Atacama Basin, and in the proximity of the Tilocalar South volcano (Tilo - 23º 58,030' S; 068º 08,529' W; 2896; 2,896 m.a.s.l.) (Fig. S1). This area is characterized by a north-south (N-S) depression, east of the Cordon de Lila range, with several subparallel N-S trending ridges culminated by Pliocene Tucucaro ignimbrite (Gardeweg and Ramírez, 1982;González et al., 2009). The lava flow from the Tilocalar South volcano emanated in a single event directly to the east of a N-S oriented fold scarp (González et al., 2009; Kuhn, 2002). Rhyolite rocks in this area were covered with a gypsum crust. Chasmoendolithic colonization in the contact zone between the gypsum cover and the rhyolite rock was distinctly detected but only in a very small number of rocks. Several pieces of rocks with apparent colonization were collected within a $1m^2$ area.

In 2010 and 2011, calcite rocks were collected near the Valle de la Luna area (Luna - 22° 54,881' S; 068° 15,211' W; 2613 m.a.s.l.) located in the north end of the Cordillera de la Sal in the northwest of the village of San Pedro de Atacama (Fig. S1). In this area, the Cordillera de la Sal is partially covered by lacustrine and piedmont deposits (silts and sands) belonging to Pliocene Vilama Formation (2.0 ± 0.9 Ma) (Naranjo et al., 1994). Laminated calcite layers were randomly distributed within the sampling area with a small number of calcite layers revealing signs of microbial colonization. We collected samples from two sites 50 m from each other.

All collected rocks were stored in sealed sterile Whirlpacks at room temperature until laboratory analysis and microscopy examination and stored at -80°C for molecular studies.

1.2 X-ray diffraction (XRD) and X-ray fluorescence spectroscopy (XRF) analyses

We used X-ray powder diffraction (XRD) on a Philips X'Pert diffractometer with graphite-monochromated CuKα radiation to identify the mineralogical composition of the Tilo and Luna rocks (ten samples for each site). The XRD patterns were obtained from random powder mounts. For qualitative analysis of the crystalline phases present in the sample, the Power Diffraction File (PDF-2, 1999) of the International Centre for Diffraction Data (ICDD) was used. A semi-quantitative analysis of these phases was performed using the normalized RIR method (Chung, 1974) and the reference intensity ratio (RIR) values for each phase given by the powder diffraction database (International Centre for Diffraction Data, ICDD). For the quantitative determinations of major and minor elements of rhyolite and calcite rocks, we used X-ray fluorescence spectrometry (XRF) on pressed-powder pellets. The Kα lines were measured on a Philips PW-1404 spectrometer equipped with a Sc-Mo x-ray tube and a scintillation gas (PR-10) detector. Super-Q Manager Geostandars (CRNS, France) analytical software was used for data analysis.

1.4 Environmental data acquisition

The Onset HOBO® Weather Station Data Logger (H21-001) used to collect microclimate data in situ over almost two years, from January 2010 to January 2012, was connected to

a SolarStream® solar-powered transmitter for data transmission by the Iridium Satellite Constellation. This weather station was located 3 km to the west of the Tilocalar sampling site. All sensors were set to take measurements every 30 min. Recorded data included air relative humidity (RH) and temperature (T) recorded 25 cm above the rock surface (the probe was shaded from the sun) using RH/T sensors (HOBO® S-THB-M002; precision, ±2.5% of RH and ±0.2ºC of T). Solar flux was measured using a photosynthetically active radiation (PAR) sensor for wavelengths of 400–700 nm (measurement range 0–2700 μmol m^{-2} s^{-1}). PAR data was also indicative of cloud cover and fog events at the sampling site. Rainfall was monitored using a Rain-o-Matic 100 (PRONAMIC ApS, Herning, Denmark) tipping bucket gauge (resolution of 1 mm). The presence of liquid water on the rhyolite rock surface was determined by a 12-bit voltage input adapter (HOBO S-VIA-CM14) interfaced with a sensor providing VDC signals to act as a smart sensor with the HOBO data logger according to procedure by (Wierzchos et al., 2012). Briefly, as external sensors, we used two 10 mm-long platinum wires (diameter 0.8 mm) positioned in parallel 10 mm apart, and tightly fixed to the rock surface with their ends attached to the rock by epoxy resin. These wires were connected to the trigger source input adapter gate. The occurrence of liquid water on the rock surface was recorded as a rise in electrical conductivity (EC), assuming that the smallest quantity of liquid water in the system would produce a voltage increase from its baseline value. Similar sensing of liquid water on the rock surface has been reported elsewhere (Omelon et al., 2006). We estimated that readings from these EC sensors are indicative of wet/dry conditions on the rock surface.

Annual rainfall precipitation data (years 1960-1980), temperature and relative humidity data (1973-1976) was obtained from historic records for the weather station located in San Pedro de Atacama village, which was located 5 km to the east of the Valle de la Luna sampling site [sources for T and RH data: Dirección General de Aguas (1977) Investigación de Recursos Hídricos en el Norte Grande and for rainfall data: Dirección General de Aguas (1987) Balance Hídrico de Chile, Ministerio de Obras Públicas].

1.4 Petrographic microscopy

Petrography studies of thin sections (30 μm-thick) of rhyolite and calcite rocks were conducted using a Nikon Eclipse LV100Pol polarized light microscope equipped with a Nikon DS-Fi1 digital camera.

1.5 Scanning electron microscopy

Scanning electron microscopy in backscattered electron mode (SEM-BSE) observation and⁄or energy dispersive X-ray spectroscopy (EDS) microanalysis were used to characterized the colonized rock samples (Wierzchos and Ascaso, 1994). As the intensity of the BSE signal depends on the mean atomic number of the sample, the SEM-BSE technique enables inorganic features to be distinguished and also identifies heavy metal-stained ultrastructural elements of living material. By *in situ* visualization of ultrastructural cell structures, different types of microorganisms and their spatial relationships can be distinguished. SEM-BSE was then used in combination with EDS to characterize the minerals associated with specific cell aggregates. For this analysis, the colonized rocks were cut transversely and fixed with 3% glutaraldehyde, in 0.1 M cacodylate buffer and subsequently stained using a 1% OsO_4 solution in 0.05 M cacodylate buffer. After fixing, the samples were dehydrated in a series of ethanol solutions, embedded in LR-White resin, and fine-polished after polymerization. The fine-polished surfaces of the rock sample cross-sections were carbon coated and examined using a DMS 960 Zeiss SEM equipped with a four-diode, semiconductor BSE detector and X-ray EDS microanalytical system (Link ISIS Oxford). The microscope and microanalytical operating conditions were as follows: 0º tilt angle, 35º X-ray take-off angle, 15 kV acceleration potential, 15 mm of working distance and 1–5 nA specimen current range.

Scanning electron microscopy in secondary electron mode (SEM-SE) was used with small chip of rocks showing endolithic colonization and maintained in an environment of 100% relative humidity (RH) during the night. Observation was performed under low vacuum using a SEM from FEI Inspect S (FEI, Eindhoven, The Netherlands) in secondary electron mode (SE) at a 15 kV acceleration potential, 10.3 mm working distance and 1–5 nA specimen current.

1.6 Fluorescence microscopy

Small chips of Luna rocks showing distinct signs of endolithic colonization (green layer beneath the surface) were crushed and suspended in double-distilled water. These suspensions were vortexed for 5 min and after 1 min of sedimentation the supernatant was centrifuged for 12 min. at x 18,000 g. The resulting pellet was stained with 20 mL of SYBR Green I (SBI) (Molecular Probes). Bright field images, SYBR Green fluorescence (green signal), and photosynthetic pigments autofluorescence (red signal) were visualized with a Zeiss AxioImager D1 fluorescence microscope equipped with Plan-Apo 60x / 1.4 Zeiss oil-immersion objective. Specific sets of filters: DAPI (Zeiss Filter Set 49; Ex/Em: 365/420-470 nm), eGFP (Zeiss Filter Set 38; Ex / Em: 450–490 / 500–550 nm) and rhodamine (Zeiss Filter Set 20; Ex / Em: 540–552 / 567–647 nm) were used for green and red signal visualization, respectively. Images were recorded with a CCD Axiocam HRc (Zeiss) camera and AxioVision 4.7 (Zeiss) software. Additional observations were made with a fluorescence microscope in structural illumination microscopy mode (SIM) (Wierzchos et al., 2011).

1.7 Transmission Electron Microscopy (TEM)

Rocks with microbial colonization were moistened with distilled water overnight before the following operations. Green spots containing chasmoendolithic microorganisms from freshly fractured rocks were gently scraped into vials with 3% glutaraldehyde in 0.1M cacodylate buffer and incubated at 5°C for 3 hours. The cells were then washed three times in cacodylate buffer, postfixed in 1% osmium tetroxide for 5 hours before being dehydrated in a graded series of ethanol and embedded in Spurr resin. Ultrathin sections were stained with lead citrate and observed in a Zeiss EM910 transmission electron microscope equipped with Gatan CCD camera.

1.8 DNA extraction, PCR-amplification, and 454 barcoded pyrosequencing

Rock samples were ground with a sterilized drill bit using a Dremel power tool (Robert Bosch Tool Corporation, Racine, WI) under aseptic conditions. Total genomic DNA was extracted from the rock powder using the PowerSoil DNA Isolation kit (MoBio Laboratories Inc., Solana Beach, CA) following the manufacturer's instructions. All sample manipulations and nucleic acid extractions were carried out in a laminar flow hood (AirClean Systems, Raleigh, NC) and all materials and reagents were either filter

sterilized, autoclaved, or UV irradiated to prevent contamination. Two DNA extractions were performed with two Luna Rock samples (Luna 1 and Luna 2) collected 50m from each other. Because of the small amount of material available, we performed one DNA extraction using several Tilo rocks collected within a $1m^2$ area. Control DNA extractions (no sample added) were performed in parallel for all environmental samples. DNA was amplified using the barcoded Universal primers 27F and 338R for the V1–V2 hypervariable region of the 16S rRNA gene. The amplification reaction mixture (25 µl) contained 200 µM deoxynucleoside triphosphates (dNTPs) each, 0.3 µM (each) primer, 1-5 ng/µl of DNA template, 0.02 U/µl of Phusion High-Fidelity DNA polymerase (New England BioLabs, Ipswich, MA), 1 x Phusion PCR buffer HF, 0.5 mM $MgCl_2$, and 3% DMSO. PCR conditions were 1 initial cycle of 30 seconds at 98°C, followed by 25 cycles of 10 seconds at 98°C, 15 seconds at 55°C, and 15 seconds at 72°C, and with a final step of 10 min. at 72°C, using a T3000 Thermal Cycler (Biometra, Horsham, PA). Amplifications of control DNA extractions were performed with the same amount of template as the environmental DNA and were all negative. Amplicons from at least 3 amplification reactions were pooled together, purified with the AMPure Kit (Agencourt, Beckman Coulter Genomics, Danvers, MA), and equimolar amounts (100 ng) of all amplicons were mixed in a single tube and sequenced by 454 pyrosequencing using a Roche GS-FLX sequencing system (Roche-454 Life Sciences, Branford, CT) by the Genomics Resource Center (GRC) at the Institute for Genome Sciences (IGS), University of Maryland School of Medicine using protocols recommended by the manufacturer as amended by the GRC.

1.9 Processing of pyrosequencing data and statistical analysis

Sequence processing and analysis was performed with CloVR-16S, which contains a series of tools for sequence analysis assembled into automated pipelines (Angiuoli et al., 2011). In a first step, all sequences were trimmed before the first ambiguous base pair. The QIIME software package (Caporaso et al., 2010b) was used for quality control of the remaining sequence reads using the split-library.pl script and the following criteria: 1) minimum and maximum length of 200 bp and 400 bp; 2) an average of q25 over a sliding window of 25 bp. If the read quality dropped below q25 it was trimmed at the first base pair of the window and then reassessed for length criteria; 3) a perfect match to a barcode

sequence; 4) a match to *E. coli* 16S rRNA gene and 5) presence of the 338R 16S primer sequence used for amplification. Sequences were binned based on sample-specific barcode sequences and trimmed by removal of the barcode and primer sequences (forward if present and reverse). Resulting sequences had a average length of 340 bp. High quality sequence reads were first de-replicated using 99% similarity using the UCLUST software package (Edgar, 2010) and detection of potential chimeric sequences was performed using the UCHIME component of UCLUST (Edgar et al., 2011) with the *de novo* algorithm. Chimeric sequences were removed prior to taxonomic assignments. Taxonomic assignments were performed as described by Ravel et al. (Ravel et al., 2011) using the RDP Naïve Bayesian Classifier (version 10.28) (Wang et al., 2007) and a confidence probabilistic threshold of 0.5 as recommended by (Claesson et al., 2009).

Operational Taxonomic Units (OTUs) were defined as clusters of sequence reads with at least 95% sequence identity; clustering was performed with Uclust (Edgar et al., 2011). Representative sequences of each OTU were then aligned with PyNAST (Caporaso et al., 2010a) against the Greengenes core set (DeSantis et al., 2006). Aligned sequences were used to generate a phylogenetic tree with FastTree (Price et al., 2010) for beta-diversity metrics using UniFrac (Lozupone et al., 2006; Hamady et al., 2010). The UniFrac significance test (Lozupone et al., 2006) was used to assess the phylogenetic differences between communities. Principal Coordinate Analysis (PCoA) plots were generated using phylogenetic distance-based weighted and unweighted UniFrac analysis (Lozupone et al., 2006). Richness, diversity estimators, and percentage of coverage by the Good's method were calculated based on OTUs with Mothur (Schloss et al., 2009). To enable accurate estimates of species richness and diversity between samples (Lozupone et al., 2011), random subsets of all datasets simulating the same sequencing effort as for the Luna 1 sample (2,622 sequences) were produced and re-analyzed (Gilbert et al., 2009). Non-metric multidimensional scaling of Theta-YC distances, based on relative abundance of OTUs, and analysis of molecular variance on the distances were performed with Mothur (Schloss et al., 2009).

References

Angiuoli, S., Matalka, M., Gussman, A., Galens, K., Vangala, M., Riley, D., Arze, C., White, J., White, O., and Fricke, W. F.: CloVR: A virtual machine for automated and portable sequence analysis from the desktop using cloud computing, BMC Bioinformatics, 12, 356-, 2011.

Caporaso, J. G., Bittinger, K., Bushman, F. D., DeSantis, T. Z., Andersen, G. L., and Knight, R.: PyNAST: a flexible tool for aligning sequences to a template alignment, Bioinformatics, 26, 266-267, 2010a.

Caporaso, J. G., Kuczynski, J., Stombaugh, J., Bittinger, K., Bushman, F. D., Costello, E. K., Fierer, N., Pena, A. G., Goodrich, J. K., Gordon, J. I., Huttley, G. A., Kelley, S. T., Knights, D., Koenig, J. E., Ley, R. E., Lozupone, C. A., McDonald, D., Muegge, B. D., Pirrung, M., Reeder, J., Sevinsky, J. R., Turnbaugh, P. J., Walters, W. A., Widmann, J., Yatsunenko, T., Zaneveld, J., and Knight, R.: QIIME allows analysis of high-throughput community sequencing data, Nat Methods, 7, 335-336, 2010b.

Chung, F. H.: Quantitative interpretation of X-ray-diffraction patterns of mixtures, J . App Crystall, 7, 526-531, 1974.

Claesson, M. J., O'Sullivan, O., Wang, Q., Nikkilä, J., Marchesi, J. R., Smidt, H., de Vos, W. M., Ross, R. P., and O'Toole, P. W.: Comparative Analysis of Pyrosequencing and a Phylogenetic Microarray for Exploring Microbial Community Structures in the Human Distal Intestine, PLoS ONE, 4, e6669, 2009.

DeSantis, T. Z., Hugenholtz, P., Larsen, N., Rojas, M., Brodie, E. L., Keller, K., Huber, T., Dalevi, D., Hu, P., and Andersen, G. L.: Greengenes, a chimera-checked 16S rRNA gene database and workbench compatible with ARB, Appl Environ Microbiol, 72, 5069-5072, 2006.

Edgar, R. C.: Search and clustering orders of magnitude faster than BLAST, Bioinformatics, 26, 2460-2461, 2010.

Edgar, R. C., Haas, B. J., Clemente, J. C., Quince, C., and Knight, R.: UCHIME improves sensitivity and speed of chimera detection, Bioinformatics, 27, 2194-2200, 2011

Gardeweg, P. M., and Ramírez, C. F.: Geología de los volcanes del Callejon de Tilocalar, Cordillera de los Andes-Antofagasta, III Congreso Geologico Chileno, Concepcion, Chile, 1982, pp. A112-A123.

Gilbert, J. A., Field, D., Swift, P., Newbold, L., Oliver, A., Smyth, T., Somerfield, P. J., Huse, S., and Joint, I.: The seasonal structure of microbial communities in the Western English Channel, Environ Microbiol, 11, 3132-3139, 2009.

González, G., Cembrano, J., Aron, F., Veloso, E. E., and Shyu, J. B. H.: Coeval compressional deformation and volcanism in the central Andes, case studies from northern Chile (23°S-24°S), Tectonics, 28, TC6003, 2009.

Hamady, M., Lozupone, C., and Knight, R.: Fast UniFrac: facilitating high-throughput phylogenetic analyses of microbial communities including analysis of pyrosequencing and PhyloChip data, ISME J, 4, 17-27, 2010.

Kuhn, D.: Fold and thrust belt structures and strike-slip faulting at the SE margin of the Salar de Atacama basin, Chilean Andes, Tectonics, 4, 1026, 2002.

Lozupone, C., Lladser, M. E., Knights, D., Stombaugh, J., and Knight, R.: UniFrac: an effective distance metric for microbial community comparison, ISME J, 5, 169-172, 2011.

Lozupone, C. A., Hamady, M., Kelley, S. T., and Knight, R.: Quantitative and qualitative beta diversity measures lead to different insights into factors that structure microbial communities, Appl Environ Microbiol, 73, 1576-1585, 2007.

Naranjo, J. A., Ramirez, C. F., and Paskoff, R.: Morphostratigraphic evolution of the northwestern margin of the Salar de Atacama basin, 23ºS-68ºW, Revista Geológica Chile, 21, 91-103, 1994.

Omelon, C. R., Pollard, W. H., and Ferris, F. G.: Environmental controls on microbial colonization of high Arctic cryptoendolithic habitats, Polar Biol, 30, 19-29, 2006.

Phoenix, V. R., Bennett, P. C., Engel, A. S., Tyler, S. W., and Ferris, F. G.: Chilean high-altitude hot-spring sinters: a model system for UV screening mechanisms by early Precambrian cyanobacteria, Geobiology, 4 15-28, 2006.

Price, M. N., Dehal, P. S., and Arkin, A. P.: FastTree 2--approximately maximum-likelihood trees for large alignments, PLoS One, 5, e9490, 2010.

Ravel, J., Gajer, P., Abdo, Z., Schneider, G. M., Koenig, S. S., McCulle, S. L., Karlebach, S., Gorle, R., Russell, J., Tacket, C. O., Brotman, R. M., Davis, C. C., Ault, K., Peralta, L., and Forney, L. J.: Vaginal microbiome of reproductive-age women, Proc Natl Acad Sci U S A, 108, 2011.

Schloss, P. D., Westcott, S. L., Ryabin, T., Hall, J. R., Hartmann, M., Hollister, E. B., Lesniewski, R. A., Oakley, B. B., Parks, D. H., Robinson, C. J., Sahl, J. W., Stres, B., Thallinger, G. G., Van Horn, D. J., and Weber, C. F.: Introducing mothur: open-source, platform-independent, community-supported software for describing and comparing microbial communities, Appl Environ Microbiol, 75, 7537-7541, 2009.

Wang, Q., Garrity, G. M., Tiedje, J. M., and Cole, J. R.: Naive Bayesian classifier for rapid assignment of rRNA sequences into the new bacterial taxonomy, Appl Environ Microbiol, 73, 5261-5267, 2007.

Wierzchos, J., and Ascaso, C.: Application of backscattered electron imaging to the study of the lichen–rock interface, J Microsc, 175, 54–59, 1994.

Wierzchos, J., Camara, B., de Los Rios, A., Davila, A. F., Sanchez Almazo, I. M., Artieda, O., Wierzchos, K., Gomez-Silva, B., McKay, C., and Ascaso, C.: Microbial colonization of Ca-sulfate crusts in the hyperarid core of the Atacama Desert: implications for the search for life on Mars, Geobiology, 9, 44-60, 2011.

Wierzchos, J., Davila, A. D., Sánchez-Almazo, I. M., Hajnos, M., Swieboda, R., and Ascaso, C.: Novel water source for endolithic life in the hyperarid core of the Atacama Desert, Biogeosciences Discuss., 9, 3071-3098, 2012.

2. Supporting figures

Fig. S1. (**a)** Location map and geomorphic units of the central part of the Atacama Desert. Rock sampling sites are indicated by open arrows (Luna and Tilo), the microweather station site used in this study (Tilocalar only) is indicated by an asterisk. The image was obtained from the 90 m Shuttle Radar Topographic Mission digital elevation model (SRTM DEM). (**b)** Sampling zone near the Tilocalar volcano (Tilo) covered by rhyolite rocks and boulders; black arrows indicate the sampling site of rhyolite covered by gypsum deposits. (**c)** Sampling area in Valle de la Luna (Luna) with sedimentary rocks; black arrows indicate the sampling site of calcite rock fragments.

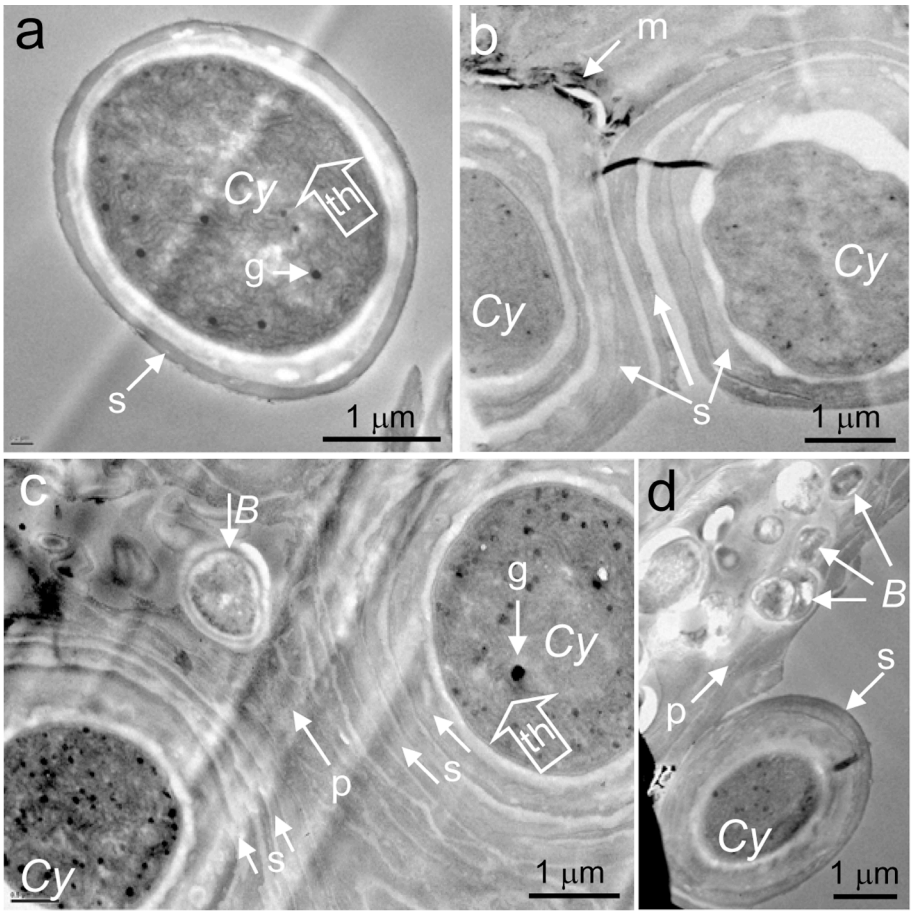

Fig. S2. TEM images of cyanobacteria cells (*Cy*) colonizing Luna calcite rock. **a)** Young baeocyte cell with cellular granules (g); open arrow indicates concentrically layered thylakoid intracytoplasmic photosynthetic membranes (th); arrow indicates cell sheath (s). **b)** Cyanobacteria (*Cy*) cells surrounded by several sheaths (s); m, unidentified mineral material is located close to the sheath. **c)** Cyanobacteria (*Cy*) cells surrounded by several concentric sheaths (s) and extracellular material (p). Within this material the heterotrophic bacteria (*B*) cell is present. **d**) TEM image shows several heterotrophic bacteria cells embedded within extracellular material (p) adhered to the cyanobacteria cell (*Cy*).

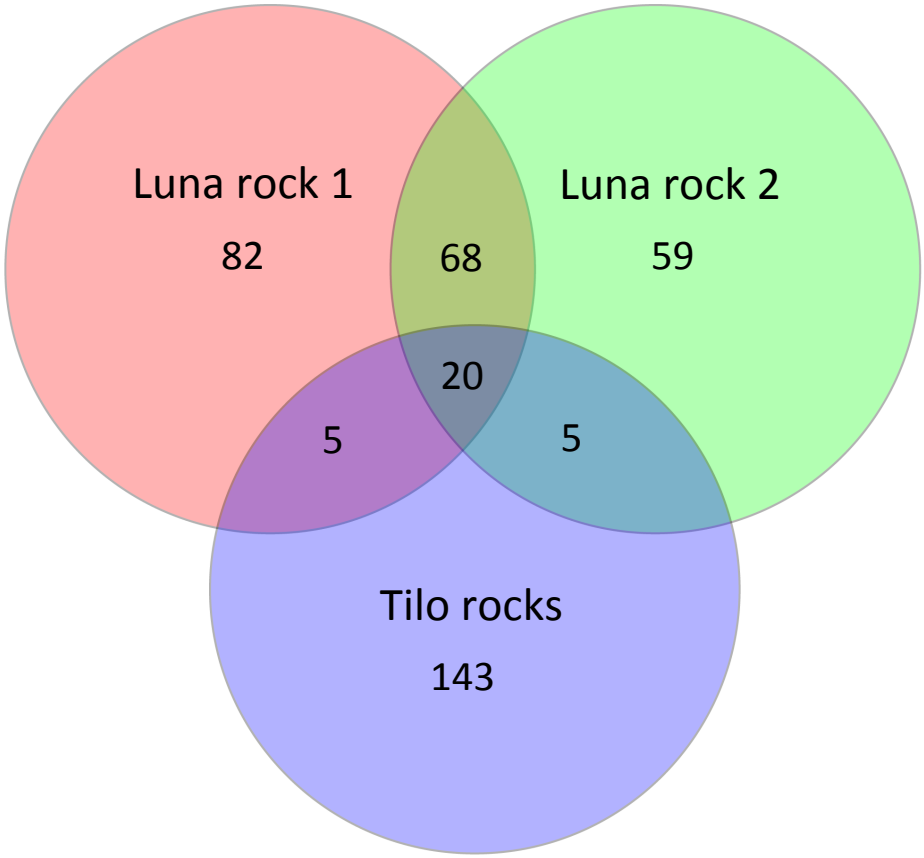

Fig. S3: Venn diagram at distance 0.05 (95% similarity level) of shared OTUs between the Luna and Tilo communities based on equally sized datasets (2,622 sequence reads). Total richness of all groups is 382; the total shared richness is 20.

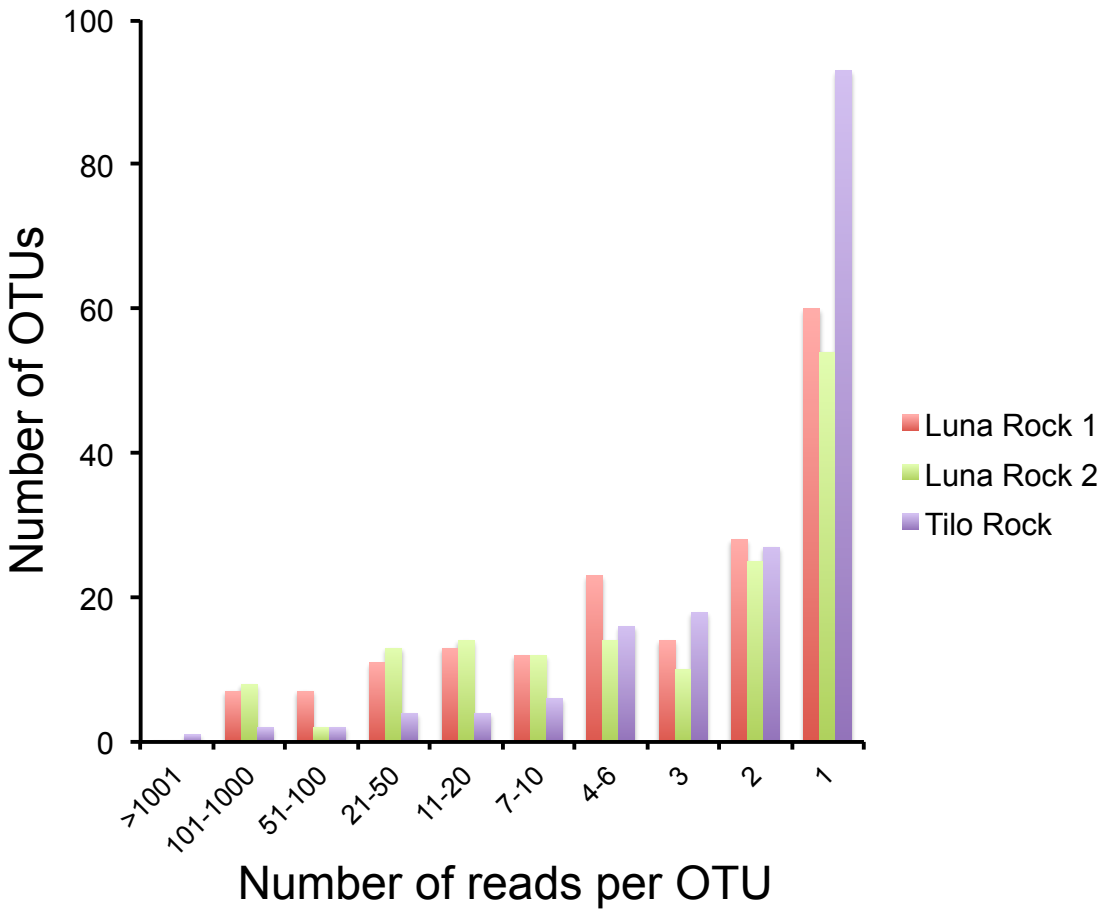

Fig. S4. OTU distribution in Luna Rock 1 and 2 and Tilo Rock samples. OTUs were assigned based on 16S rRNA gene sequences at the 95% similarity level.

Table S1. Relative abundance of major bacterial families (>10 counts summed across all samples) in the Tilo and Luna rocks

Familes	Tilo Rock	Luna Rock 1	Luna Rock 2
Cyanobacteria Other	431	989	1145
Rubrobacterales	104	444	348
Cyanobacteria GpIX	0	260	97
Bacteria Unassigned	29	187	295
Trueperaceae	3	164	50
Actinomycetales	86	139	209
Cyanobacteria GpI	1447	107	39
Gemmatimonadaceae	0	86	100
Actinobacteria Other	19	73	57
Rhizobiales Other	38	44	31
Flexibacteraceae	29	40	105
Thermomicrobiaceae	6	18	18
Methylobacteriaceae	13	7	20
Sphingomonadaceae	40	6	34
Acidimicrobiales	1	6	8
Acidobacteriaceae	7	4	3
Proteobacteria Other	15	3	4
Alphaproteobacteria Other	4	3	7
Comamonadaceae	27	1	0
Acetobacteraceae	3	1	8
Pseudomonadaceae	149	0	0
Xanthomonadaceae	42	0	0
Caulobacteraceae	19	0	4
Crenotrichaceae	6	0	7
Burkholderiales Other	9	0	3
Rhizobiaceae	11	0	0

Table S2. Taxonomic assignments for Atacama endolithic cyanobacteria

	Best BLAST hit		Best cultured BLAST hit					
OTU (Accession #)	Organism (Accession #)	% Identity	Organism (Accession #)	% Identity	Tilo % of cyanobacteria	Luna % of cyanobacteria	Cultured order subsection	Source for uncultured best BLAST hit
OTU 66 (SRR496205.4434)	Uncultured bacterium 12TCLN413 (AB637339.1)	94%	*Chroococcidiopsis* sp. str. CC3 (DQ914865.2)	91%	19.9	0	Pleurocapsales	Japan: Tottori soil
OTU 75 (SRR496205.9159)	Uncultured cyanobacterium clone AY1_2 (FJ890991.1)	95%	*Anabaena cylindrica* PCC 7122 (AF091150.1)	93%	1.5	0	Nostocales	Chile: Atacama Desert quartz
OTU 213 (SRR496207.1598)	Uncultured cyanobacterium clone AY5_1 (FJ891012.1)	95%	*Chroococcidiopsis* sp. str. CC1 (DQ914863.2)	94%	4.3	8.0	Pleurocapsales	Chile: Atacama Desert quartz
OTU 215 (SRR496207.1624)	Uncultured *Nostocales* cyanobacterium clone A1-01QJH (EU434884.1)	97%	*Phormidium murrayi* Ant-Ph58 (DQ493872.1)	90%	0	10.4	Oscillatoriales	Spain: Aragon natural shelter with prehistoric paintings
OTU 216 (SRR496207.2465)	Uncultured cyanobacterium clone AY6_6 (FJ891036.1)	99%	*Chroococcidiopsis* sp. str. CC1 (DQ914863.2)	92%	0	13.5	Pleurocapsales	Chile: Atacama Desert quartz
OTU 221 (SRR496205.8468)	*Chroococcidiopsis* sp. str. CC2 (DQ914864.2)	99%			72.7	4.5	Pleurocapsales	
OTU 275 (SRR496207.1958)	Uncultured bacterium 12TCLN413 (AB637339.1)	100%	*Anabaena* sp. SKJF11 (EU022719.1)	88%	0	9.7	Nostocales	Japan: Tottori soil
OTU 276 (SRR496207.366)	Uncultured cyanobacterium clone AY5_1 (FJ891012.1)	96%	*Anabaena cylindrica* PCC 7122 (AF091150.1)	91%	0	14.5	Nostocales	Chile: Atacama Desert quartz
OTU 277 (SRR496207.1297)	*Wollea saccata* str. ACCS 045 (GU434226.1)	92%			0	7.2	Nostocales	
OTU 289 (SRR496207.1692)	Uncultured cyanobacterium clone F27_9C_RP (EF683070.1)	96%	*Chroococcidiopsis* sp. str. CC1 (DQ914863.2)	88%	0	12.8	Pleurocapsales	Eastern Mediterranean atmosphere
OTU 304 (SRR496211.1)	Uncultured cyanobacterium clone AY5_13 (FJ891024.1)	98%	*Chroococcidiopsis* sp. str. CC1 (DQ914863.2)	91%	0	2.7	Pleurocapsales	Chile: Atacama Desert quartz
OTU 317 (SRR496211.1092)	*Chroococcidiopsis* sp. str. CC2 (DQ914864.2)	96%			0	1.1	Pleurocapsales	
OTU 343 (SRR496207.2252)	Uncultured cyanobacterium clone GG3 (JQ404415.1)	97%	*Anabaena cylindrica* PCC 7122 (AF091150.1)	92%	0	8.4	Nostocales	China: Forbidden City marble sculpture
OTU 351 (SRR496207.2647)	Uncultured cyanobacterium clone C07_ELL01 (EF220066.1)	96%	*Chroococcidiopsis* sp. str. CC1 (DQ914863.2)	91%	0	6.4	Pleurocapsales	Antarctica: Ellsworth Mountains unvegetated soil